Visualising and Quantifying Hydroxyapatite in Bone Using Confocal Fluorescence Microscopy and OsteoImage™

Dui Lan Sun, Joel Turner

Faculty of Medical Sciences, University College London (UCL), 74 Huntley Street, London WC1E 6BT, United Kingdom

1 Introduction

Hydroxyapatite is a calcium phosphate bioceramic that constitutes the mineral component of natural bone. Due to its mechanical strength, particularly under compressive loads, and its excellent osteoconductive and osteointegrative properties, hydroxyapatite is widely used in medicine and dentistry, including in bone grafts, implant coatings, and scaffolds for regenerative therapies [1,2]. Beyond its functional role, hydroxyapatite serves as a key marker of successful bone mineralisation in tissue models [3,4]. Accurate visualisation and quantification of hydroxyapatite are therefore critical for evaluating the performance of biomaterials in vitro, allowing assessment of whether mineralisation has occurred, where the mineral has deposited, and how mature or organised the mineral phase is.

This need is heightened by the global public health burden of bone fractures, particularly among individuals with osteoporosis and low bone mass, which significantly reduce quality of life, impede return to work, and often lead to social isolation, imposing substantial economic and social costs [5,6]. Consequently, there is a clear requirement for a cost-effective, fast, and reliable method to visualise and quantify hydroxyapatite in vitro, enabling more efficient testing of biomaterials, drugs, and disease mechanisms [7].

A wide range of methods is currently employed to visualise and quantify hydroxyapatite in vitro, each with specific advantages and limitations. Alizarin Red S (ARS) and Von Kossa staining are commonly used to visualise and semi-quantify mineral deposition, with ARS binding to calcium and Von Kossa to phosphate specifically. However, neither stain binds specifically to hydroxyapatite [8–11]. Furthermore, mineralised nodules only form after ~21 days of culture in osteogenic media, meaning these stains can only detect late-stage mineralisation and not earlier osteogenic events. Commercial assays are available to quantify total calcium and phosphorus concentrations within bone nodules, indirectly assessing bone formation. Nevertheless, calcium and phosphorus in cells, culture media, and bioactive glasses may introduce background signals that confound accurate interpretation [9,10,12,13]. Scanning electron microscopy (SEM) combined with energy-dispersive X-ray spectroscopy (EDX) allows high-resolution imaging and elemental analysis of mineral phases. Still, it requires dehydration and, in many cases, conductive coating, which may alter native structures or introduce artefacts [14,15]. Micro-computed tomography (μCT) enables non-destructive three-dimensional imaging of

mineral distribution but relies on X-ray attenuation and is sensitive to beam-hardening artefacts that can artificially reduce apparent density in central regions [16,17]. Phase identification methods such as X-ray diffraction (XRD), Fourier transform infrared (FTIR) spectroscopy, and Raman spectroscopy provide confirmation of hydroxyapatite crystal structure but are also limited: XRD is destructive and costly, FTIR requires experienced interpretation, and Raman analysis can fail to capture all mineral deposits, leading to underestimation of mineralisation [10,18,19].

Given these limitations, there is a clear need for an alternative approach that enables direct, specific, non-destructive, cost-effective, and straightforward visualisation and quantification of hydroxyapatite. In this study, we investigated confocal fluorescence microscopy combined with OsteoImage™, a fluorescent probe that binds exclusively to crystalline hydroxyapatite, thereby providing a specific measure of bone mineralisation [20–22]. The effectiveness of this technique was evaluated across a range of conditions, including samples fixed at different time points (days 7, 14, and 21), under low- and medium-glucose environments, with and without bioactive glasses (45S5 and CoSiBG), and in both two-dimensional and three-dimensional culture models.

2 Materials and Methods

2.1 Preparation of Cell Cultures and Bioactive Glass Substrates

2.1.2 Preparation of 2D Cultures

Two-dimensional cultures without bioactive glass were fixed at days 7, 14, and 21 under low-glucose conditions, and at day 21 under medium-glucose conditions. Two-dimensional cultures containing bioactive glass, either 45S5 or CoSiBG, were fixed at day 21, with replicates under both low- and medium-glucose conditions.

2.1.3 Preparation of 3D Cultures

Three-dimensional cultures without bioactive glass were fixed at day 21 under low-glucose conditions.

2.2 Fluorescent Labelling of Nuclei and Hydroxyapatite

All cultures were stained with OsteoImage™ (Lonza, Switzerland) to visualise hydroxyapatite deposition and with DAPI (4',6-diamidino-2-phenylindole; Thermo Fisher Scientific, USA) to label cell nuclei. Staining was carried out according to the manufacturer's protocols. Briefly, samples were fixed in 4% paraformaldehyde for 15 minutes at room temperature, rinsed three times with phosphate-buffered saline (PBS), and incubated with the OsteoImage™ staining solution for 30 minutes in the dark. Following three further PBS washes, cultures were counterstained with DAPI for 5

minutes, washed again, and mounted in PBS before confocal imaging. Stained samples were stored at 4 °C in the dark until imaging to preserve the fluorescence signal.

2.3 Confocal Laser Scanning Microscopy

Confocal microscopy allows optical sectioning of fluorescently labelled samples, capturing high-resolution images at specific depths while minimising out-of-focus light, enabling three-dimensional reconstruction of mineralised regions and nuclei. Imaging was performed on a Leica TCS SP8 confocal laser scanning microscope (Leica Microsystems, Wetzlar, Germany). DAPI was excited at 405 nm with emission collected at 461 nm, while OsteoImage™ was excited at 490 nm with emission collected at 520 nm. The pinhole was standardised to 3.09 AU for all samples, balancing optical section thickness and signal intensity while maintaining practical scan times.

Images were acquired with ×5, ×10, and ×40 lenses. The ×5 lens provided an overview of bulk mineralisation across the sample, while the ×40 lens allowed detailed visualisation of osteoblast growth and hydroxyapatite deposition at the cellular level. The ×10 lens was initially assessed but ultimately excluded as it provided no additional information beyond the ×5 overview. Optical zoom settings were 0.75× at low magnification, allowing maximum scan speed without reducing resolution, and 1.28× at high magnification, providing the highest achievable resolution without increasing scan time. Scan speed and resolution were adjusted to optimise the signal-to-noise ratio, and z-stacks were acquired to capture the full depth of mineralised structures.

3 Results

3.1 Effect of Time on Bone Mineralisation

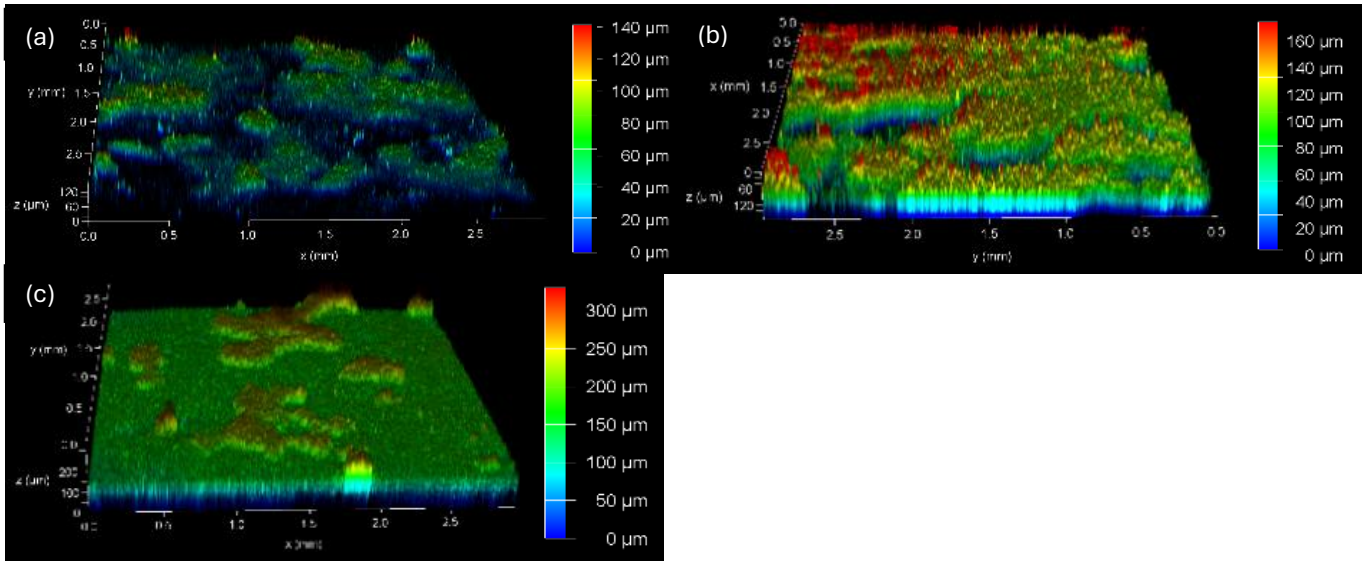

Figure 1. Hydroxyapatite with ×5 lens: (a) day 7, (b) day 14, and (c) day 21.

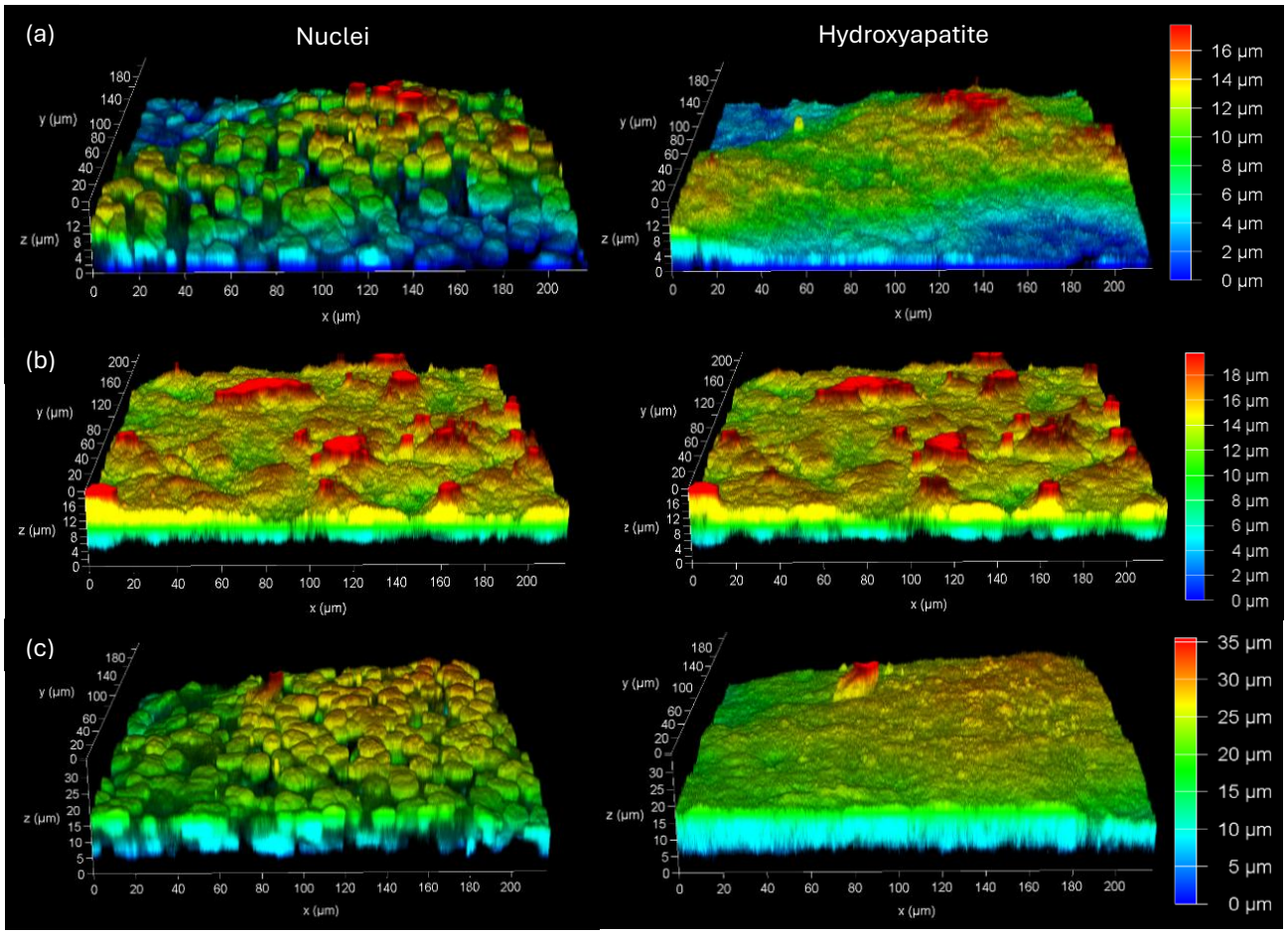

Figure 2. Nuclei and hydroxyapatite with ×40 lens: (a) day 7, (b) day 14, and (c) day 21.

Hydroxyapatite was used to directly indicate bone mineralisation, reflecting the conversion of unmineralised osteoid into mineralised bone matrix. Samples were observed with ×5 and ×40 lenses. With the ×5 lens, hydroxyapatite exhibited z-depths of 140 μm at day 7, 160 μm at day 14, and 300 μm at day 21. At ×40 magnification, nuclei and hydroxyapatite exhibited z-depths of 16 μm, 18 μm, and 35 μm at days 7, 14, and 21, respectively. Across both lenses, mineralisation increased progressively with time under low-glucose conditions.

3.2. Effect of Metabolic Environment

3.2.1 Effect of Glucose Concentration on Bone Mineralisation (Low vs. Medium Glucose)

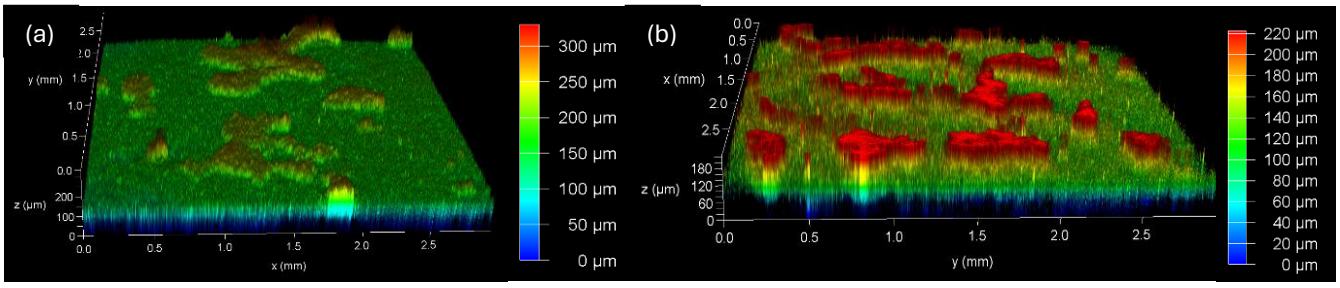

Figure 3. Hydroxyapatite with the ×5 lens at day 21: (a) low glucose and (b) medium glucose conditions.

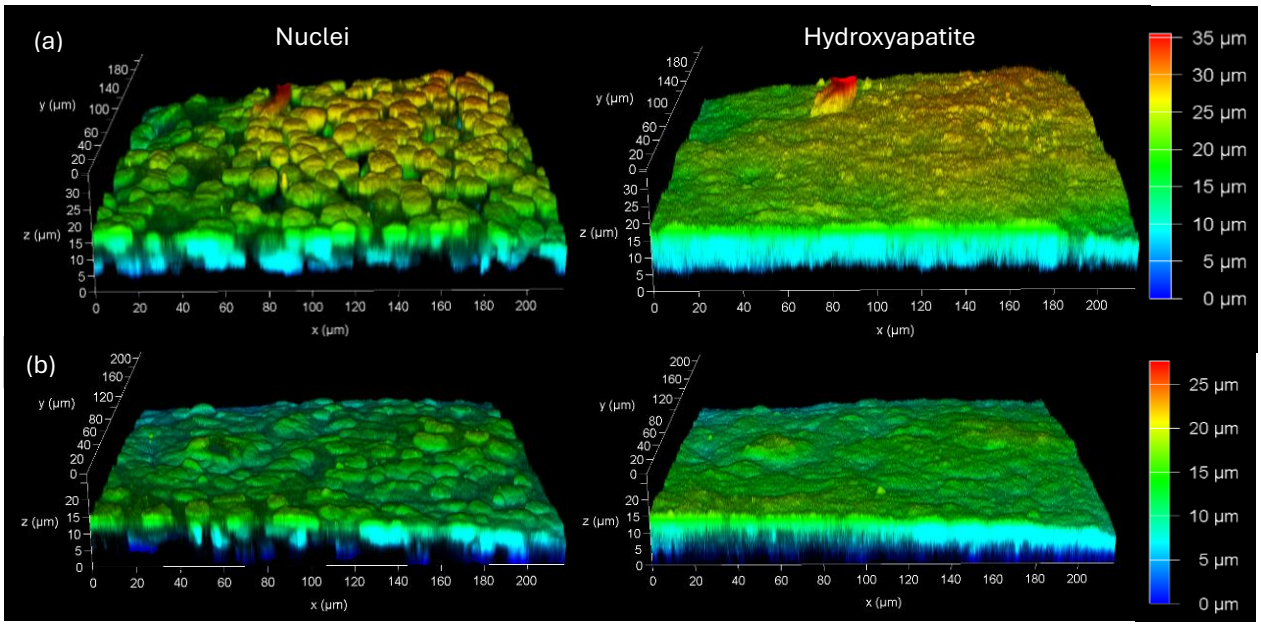

Figure 4. Nuclei and hydroxyapatite with the ×40 lens at day 21: (a) low glucose and (b) medium glucose conditions.

Bone mineralisation was assessed under low-glucose conditions, representing normal physiology, and medium-glucose conditions, representing hyperglycaemia. With the ×5 lens, hydroxyapatite exhibited z-depths of 300 µm in low-glucose conditions and 220 µm in medium-glucose conditions. With the ×40 lens, nuclei and hydroxyapatite exhibited z-depths of 35 µm and 25 µm under low- and medium-glucose conditions, respectively. Across both lenses, mineralisation was greater in low-glucose conditions compared to medium-glucose conditions.

3.2.2 Effect of Glucose Concentration on Bone Mineralisation in 45S5 Bioactive Glass and CoSiBG (Low vs. Medium Glucose)

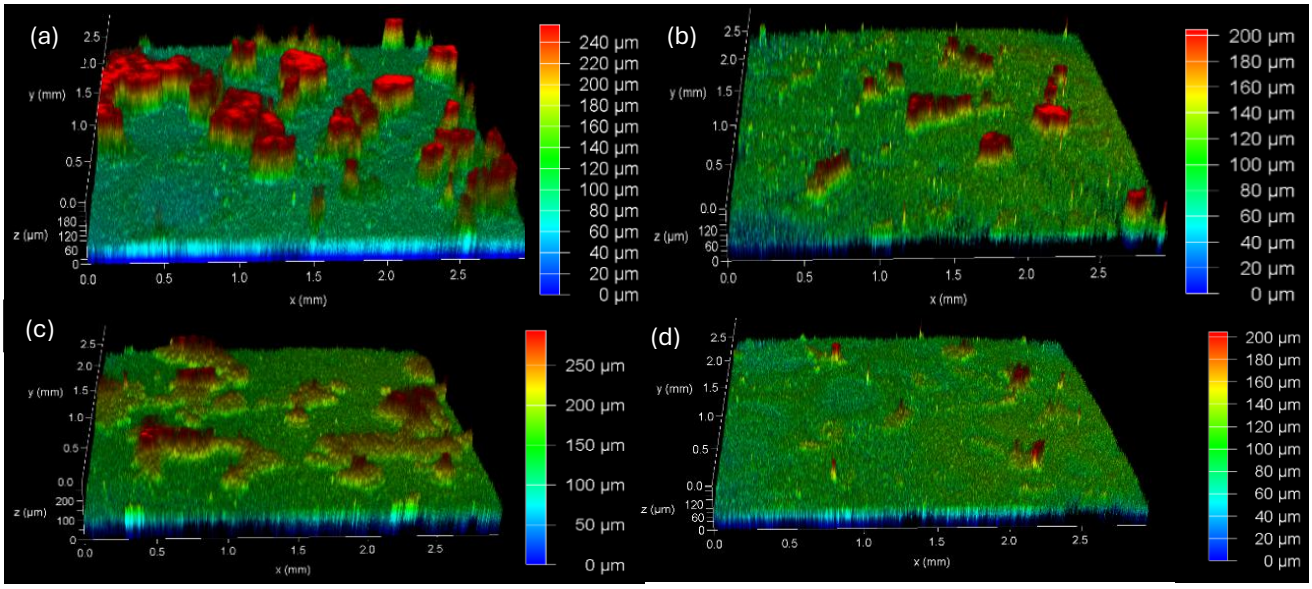

Figure 5. Hydroxyapatite with the ×5 lens: (a) 45S5 bioactive glass at day 21 under low glucose conditions, (b) 45S5 bioactive glass at day 21 under medium glucose conditions, (c) CoSiBG at day 21 under low glucose conditions, and (d) CoSiBG at day 21 under medium glucose conditions.

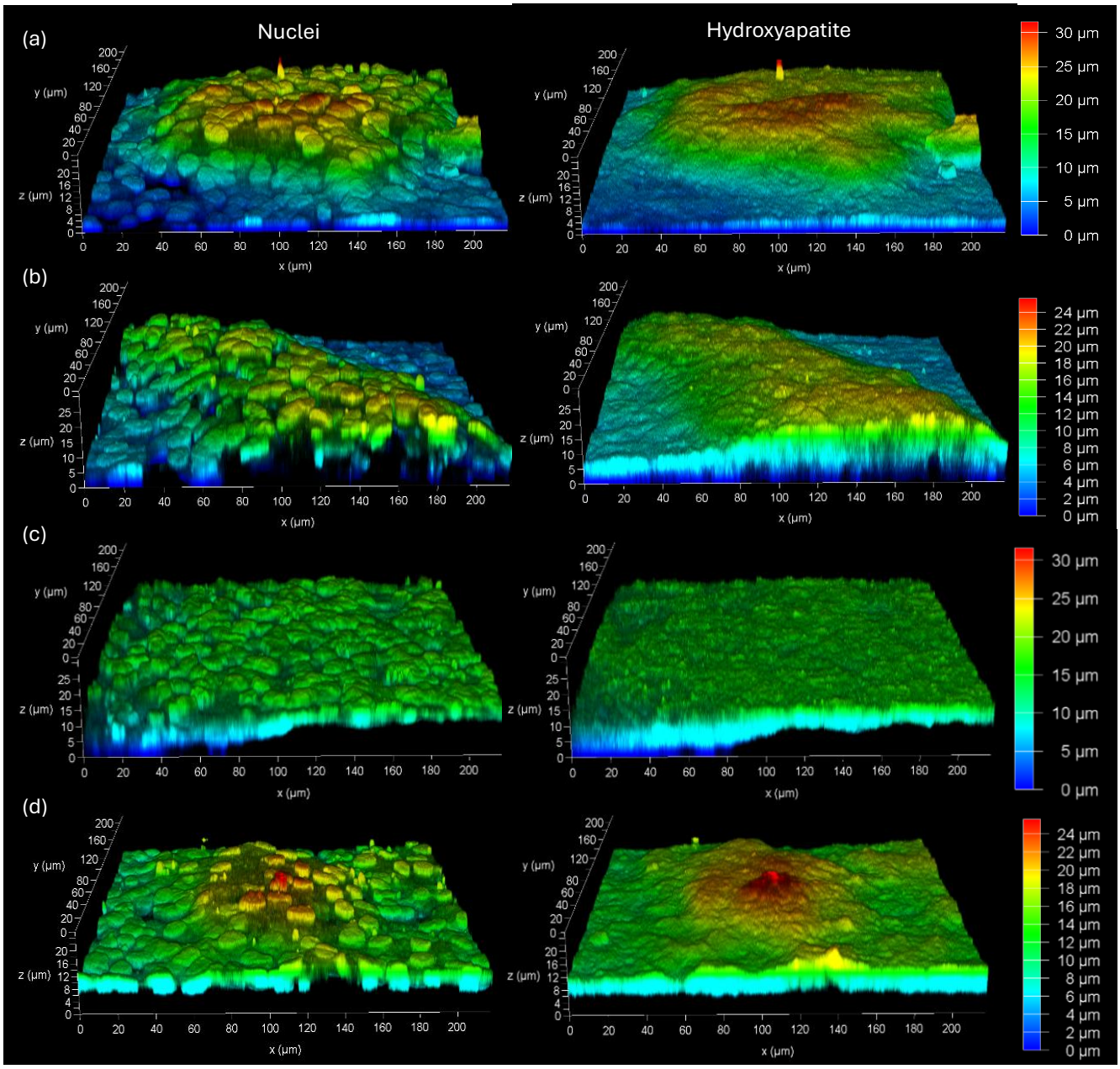

Figure 6. Nuclei and hydroxyapatite with the ×40 lens: (a) 45S5 bioactive glass at day 21 under low glucose conditions, (b) 45S5 bioactive glass at day 21 under medium glucose conditions, (c) CoSiBG at day 21 under low glucose conditions, and (d) CoSiBG at day 21 under medium glucose conditions.

With the ×5 lens, hydroxyapatite exhibited z-depths of 200 µm (medium glucose) and 250 µm (low glucose) with 45S5 bioactive glass, and 180 µm (medium glucose) and 240 µm (low glucose) with CoSiBG. With the ×40 lens, nuclei and hydroxyapatite exhibited z-depths of 24 µm (medium glucose) and 30 µm (low glucose) for both materials. Across

both lenses, mineralisation was greater in low-glucose compared to medium-glucose conditions, with slightly higher z-depths observed in 45S5 bioactive glass compared to CoSiBG.

3.3 Effect of Biomaterial Composition

3.3.1 Effect of 45S5 Bioactive Glass and CoSiBG on Bone Mineralisation in Low Glucose (Physiologic) Conditions

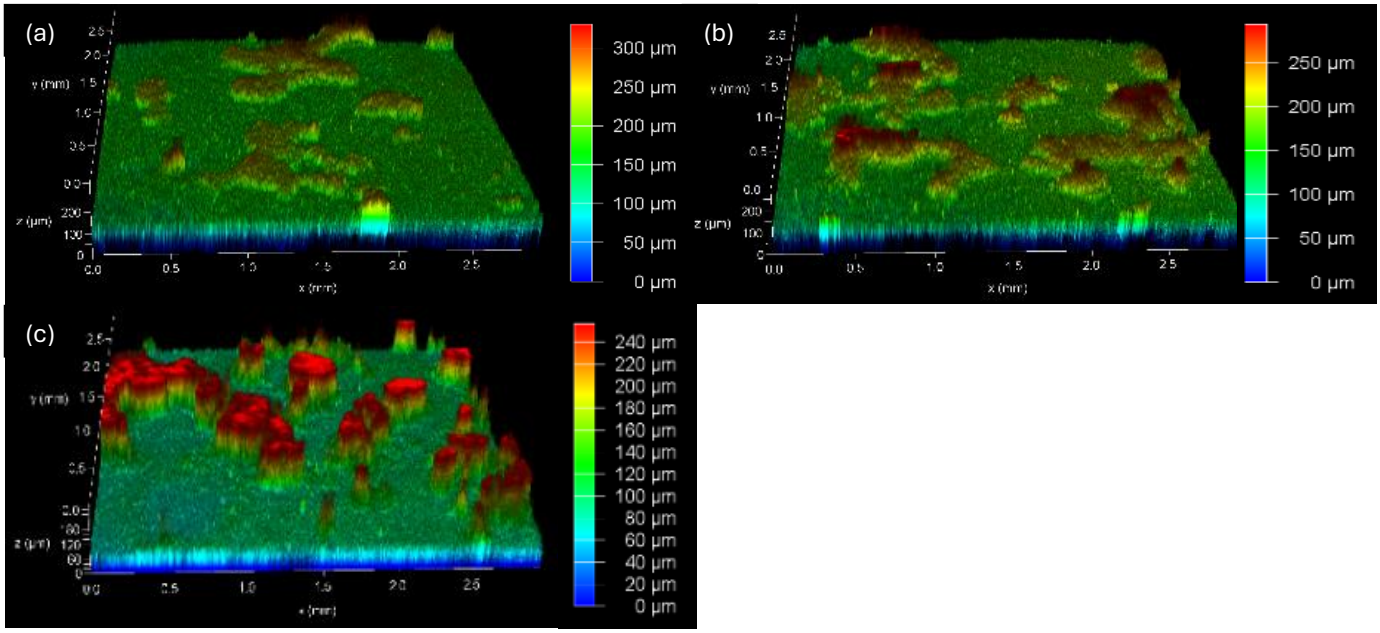

Figure 7. Hydroxyapatite with the ×5 lens under low glucose conditions at day 21: (a) Control, (b) 45S5 bioactive glass, and (c) CoSiBG.

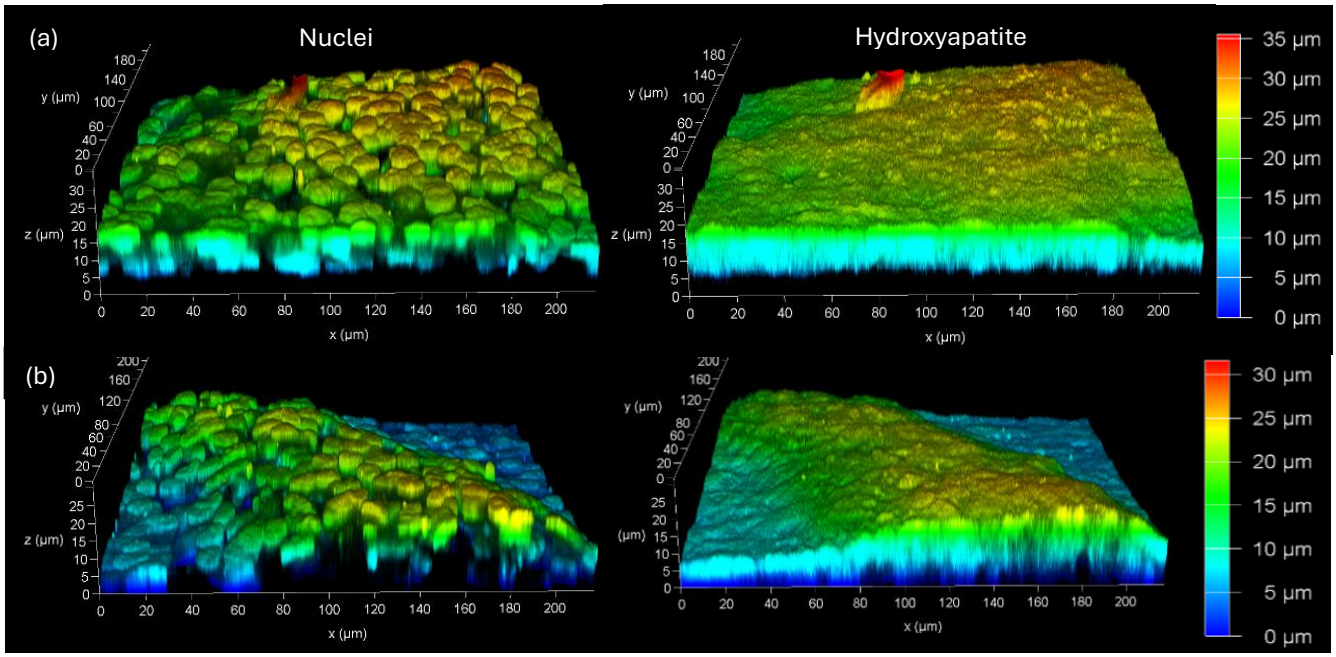

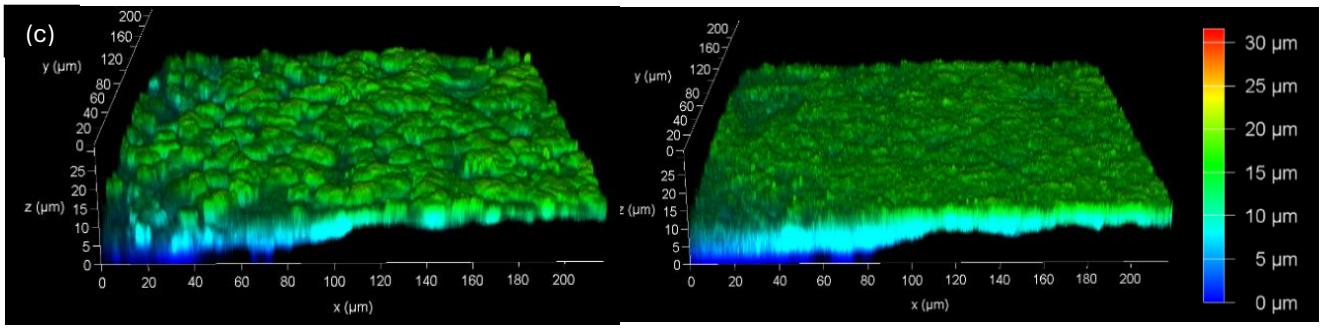

Figure 8. Nuclei and hydroxyapatite with the ×40 lens under low glucose conditions at day 21: (a) Control, (b) 45S5 bioactive glass, and (c) CoSiBG.

With the ×5 lens under low-glucose conditions, hydroxyapatite exhibited z-depths of 300 µm in the control, 250 µm in 45S5 bioactive glass, and 240 µm in CoSiBG. With the ×40 lens, nuclei and hydroxyapatite exhibited z-depths of 35 µm, 30 µm, and 30 µm in the control, 45S5 bioactive glass, and CoSiBG, respectively. Overall, mineralisation was slightly higher in the control compared to both bioactive glass groups under low-glucose conditions.

3.3.2 Effect of 45S5 Bioactive Glass and CoSiBG on Bone Mineralisation in Medium Glucose (Hyperglycaemic) Conditions

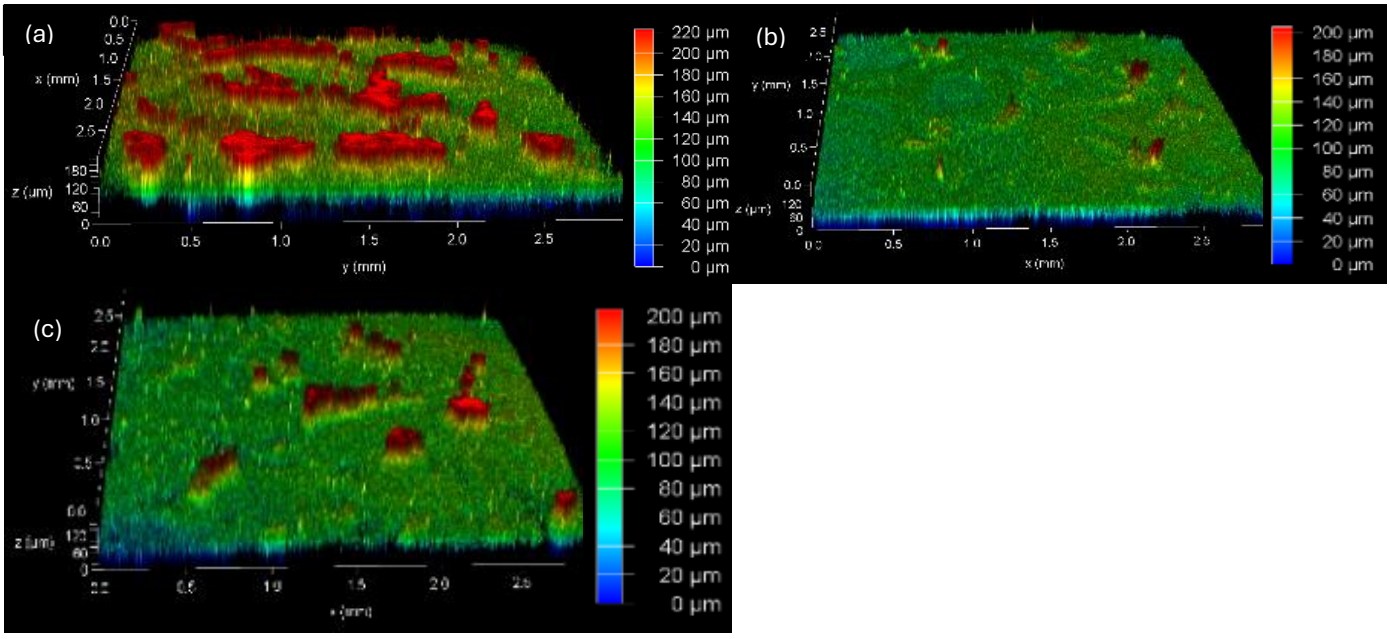

Figure 9. Hydroxyapatite with the ×5 lens under medium glucose conditions at day 21: (a) Control, (b) 45S5 bioactive glass, and (c) CoSiBG.

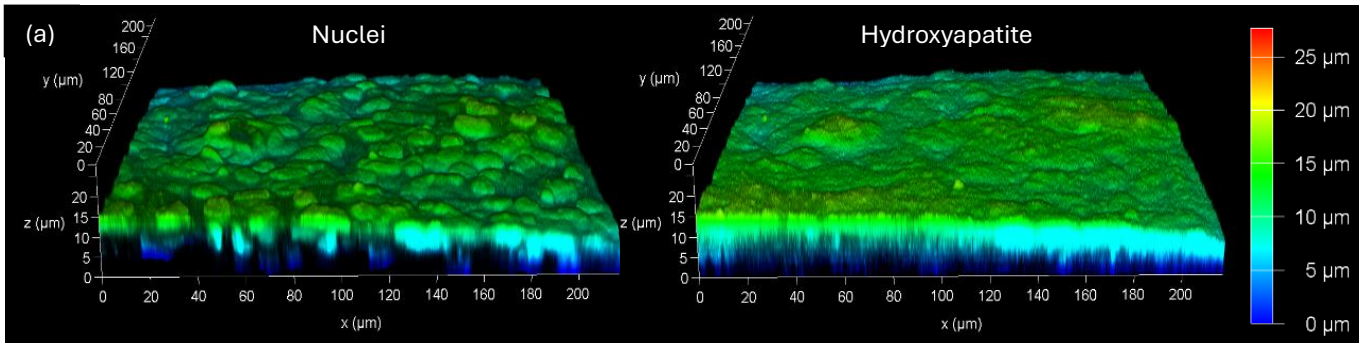

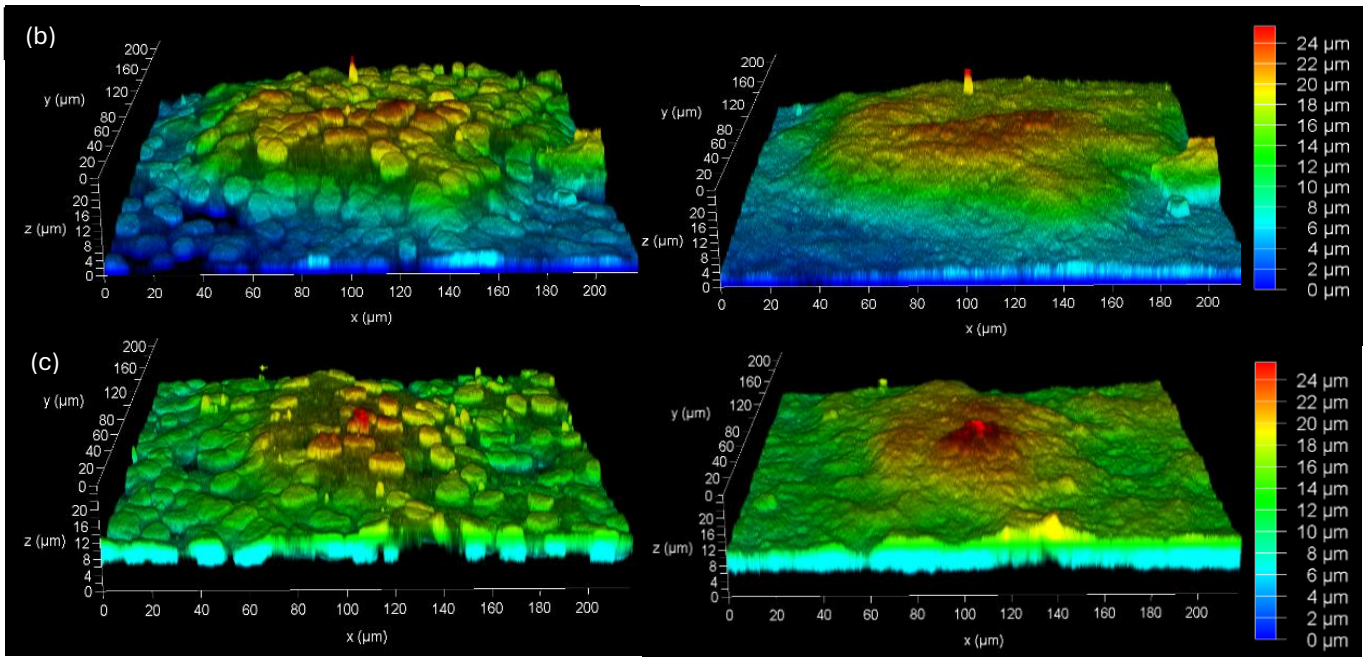

Figure 10. Nuclei and hydroxyapatite with the ×40 lens under medium glucose conditions at day 21: (a) Control, (b) 45S5 bioactive glass, and (c) CoSiBG.

With the ×5 lens under medium-glucose conditions, hydroxyapatite exhibited z-depths of 200 µm in 45S5 bioactive glass, 180 µm in CoSiBG, and 220 µm in the control. With the ×40 lens, nuclei and hydroxyapatite exhibited z-depths of 24 µm, 24 µm, and 25 µm in 45S5 bioactive glass, CoSiBG, and the control, respectively. Overall, mineralisation in medium-glucose conditions was slightly reduced in both bioactive glass groups compared to the control.

3.3.3 Comparison of 45S5 Bioactive Glass and CoSiBG

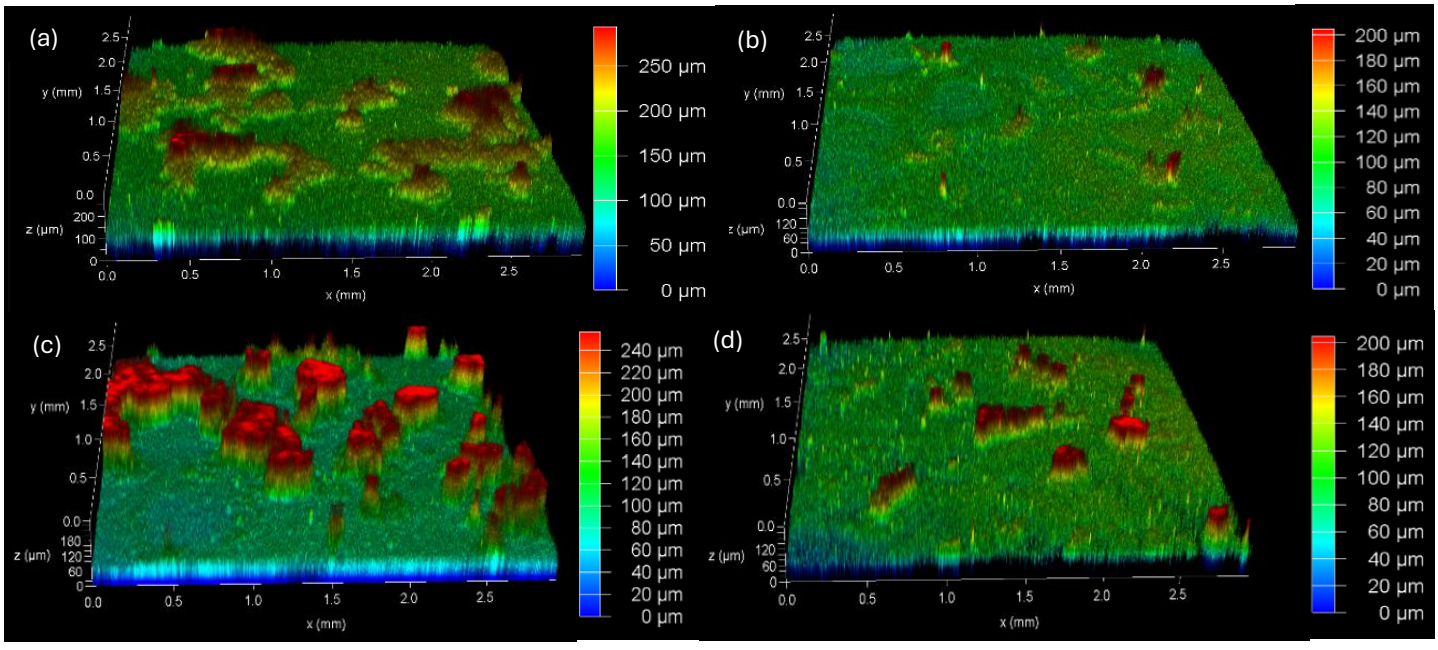

Figure 11. Hydroxyapatite with the ×5 lens: (a) 45S5 bioactive glass at day 21 under low glucose conditions, (b) 45S5 bioactive glass at day 21 under medium glucose conditions, (c) CoSiBG at day 21 under low glucose conditions, and (d) CoSiBG at day 21 under medium glucose conditions.

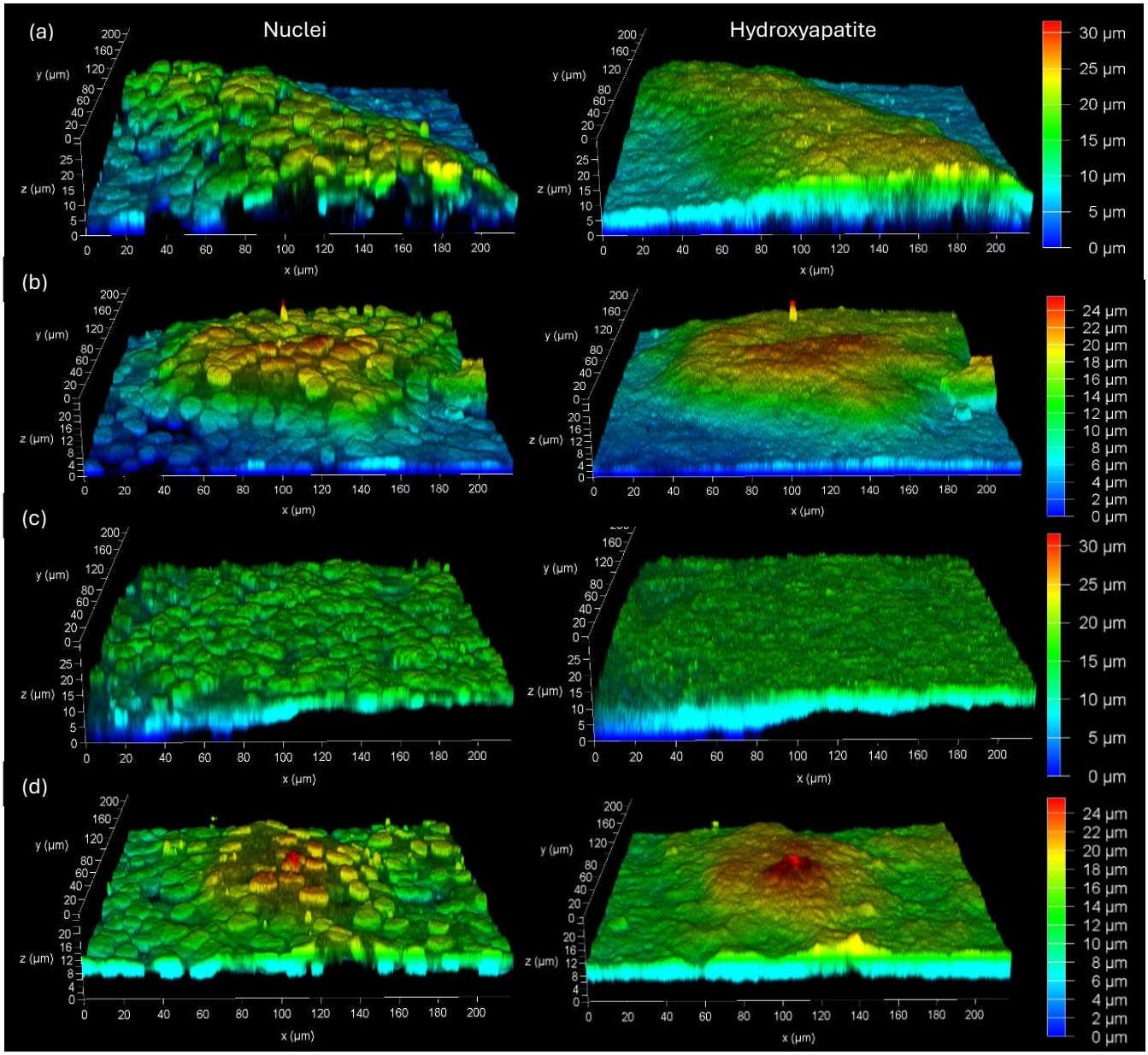

Figure 12. Nuclei and hydroxyapatite with the ×40 lens: (a) 45S5 bioactive glass at day 21 under low glucose conditions, (b) 45S5 bioactive glass at day 21 under medium glucose conditions, (c) CoSiBG at day 21 under low glucose conditions, and (d) CoSiBG at day 21 under medium glucose conditions.

With the ×5 lens, 45S5 bioactive glass exhibited greater hydroxyapatite z-depths than CoSiBG under both medium-glucose (250 vs. 240 µm) and low-glucose conditions (200 vs. 180 µm). With the ×40 lens, nuclei and hydroxyapatite z-depths were the same for both 45S5 bioactive glass and CoSiBG under medium-glucose (24 µm) and low-glucose

conditions (30 µm). Overall, 45S5 bioactive glass promoted slightly greater mineralisation than CoSiBG at lower magnification, while at higher magnification, mineralisation was comparable between the two materials.

3.4 Effect of Culture Dimensionality (2D vs. 3D Cultures)

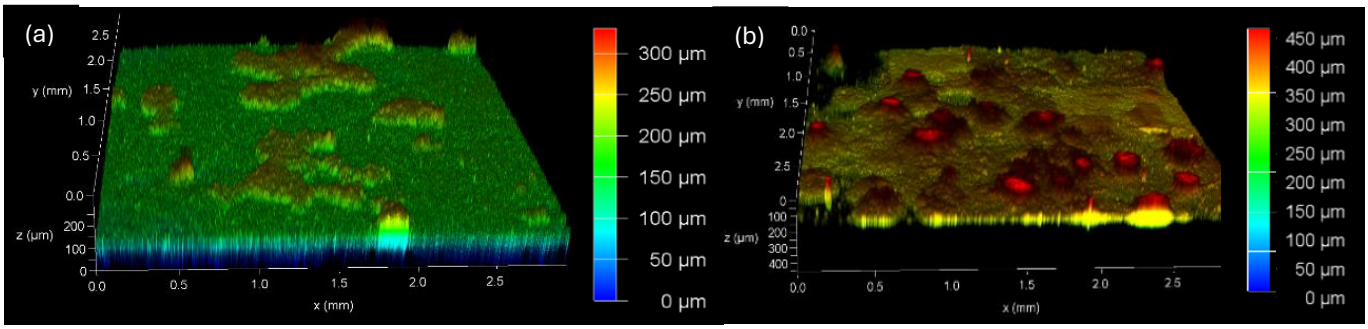

Figure 13. Hydroxyapatite with the ×5 lens at day 21: (a) 2-dimensional, (b) 3-dimensional.

Bone mineralisation was assessed in 2D and 3D cultures. With the ×5 lens, hydroxyapatite exhibited a z-depth of 300 µm in 2D culture (control) and 450 µm in 3D culture.

4 Discussion

4.1 Evaluation of the Hydroxyapatite Visualisation and Quantification Technique

4.1.1 Overview of Technique Application

Confocal fluorescence microscopy, combined with the OsteoImage™, which binds specifically to hydroxyapatite, was employed as a technique to visualise and quantify bone mineralisation.

4.1.2 Imaging Parameters and Magnification Considerations

Pinhole size was standardised to 3.09 AU across all samples. This value provided an optimal balance between axial resolution and signal intensity, allowing each scan to be completed in under one hour while minimising background noise that could interfere with hydroxyapatite detection.

Samples were imaged with ×5, ×10, and ×40 lenses. The ×5 lens provided the widest field of view, enabling visualisation of overall mineral deposition patterns and growth across the sample. The ×40 lens allowed detailed assessment of osteoblast behaviour and hydroxyapatite deposition at the cellular level. The images taken with the ×10 lens were excluded, as they did not provide additional information beyond ×5 and captured a smaller portion of the sample. Imaging with the ×5 and ×40 lenses allowed both global and local quantification of bone mineralisation.

Optical zoom was adjusted to two main settings: 0.75 and 1.28. With the ×5 lens, 0.75× zoom provided sufficient resolution for overall pattern analysis while maximising scan speed. With the ×40 lens, the 1.28× zoom allowed the maximum achievable resolution without increasing scan time, enabling detailed assessment of cellular-level mineralisation. Overall, imaging parameters were optimised to balance resolution and speed, using lower resolution for wide-field scans and higher resolution for detailed cellular analyses.

4.1.3 Advantages of the Technique

This technique primarily involves using z-stacks and fluorescence, which are relatively inexpensive, widely available, and straightforward to learn. Scans can be completed quickly, often within one hour per sample. A trade-off exists between speed and resolution: faster scans typically require lower resolution. However, this compromise is acceptable, particularly at lower magnifications, where the objective is to obtain an overview of bone nodule formation across the dish rather than focus on fine structural details. Even at smaller fields of view where higher resolution is required, scans can still be completed within an hour due to the limited imaged area. At very high magnifications and resolutions, the technique allows detailed observation of osteoblast interactions, cell growth patterns, and the initial sites of hydroxyapatite deposition, providing insights into the dynamics of bone mineralisation at the cellular level. This technique provides quantitative three-dimensional visualisation and, in addition, reveals distinct layers of cells and hydroxyapatite, enabling detailed assessment of their interactions.

OsteoImage™ binds specifically to hydroxyapatite, allowing a precise assessment of osteogenic mineralisation [20]. This specificity provides insight into osteogenesis at both early and late stages, rather than being limited to endpoint assessment [21–23].

4.1.4 Limitations and Sources of Error

When using fluorescence, the beginning of a nodule is typically identified as the first detectable signal, and the end as the last signal, but distinguishing the actual nodule from background noise at the top and bottom can be difficult. Furthermore, it is not possible to standardise the start and end points of z-stacks across different nodules, introducing potential human error.

4.2 Interpretation of Observed Mineralisation

4.2.1 Effect of Time on Bone Mineralisation

The progressive increase in hydroxyapatite z-depth over time reflects the normal progression of osteogenesis, where osteoblasts first deposit an unmineralised collagen matrix that subsequently undergoes mineral deposition. This temporal pattern is consistent with physiological bone development, in which mineralisation is a time-dependent process that gradually converts osteoid into mature mineralised tissue. The

findings confirm that the culture system supported sustained bone-like matrix maturation under low-glucose conditions.

4.2.2 Effect of Metabolic Environment

4.2.2.1 Effect of Glucose Concentration on Bone Mineralisation (Low vs. Medium Glucose)

The greater mineralisation observed under low-glucose conditions compared to medium-glucose conditions is consistent with the expected effects of glucose availability on bone formation. Under normal physiological glucose levels, osteoblasts can function efficiently. In contrast, hyperglycaemia has been shown to impair osteoblast function and mineralisation [24–27]. Hyperglycaemia also promotes bone resorption largely through the accumulation of advanced glycation end products and the generation of reactive oxygen species [26–29]. These findings therefore reinforce that physiological glucose levels favour normal bone mineralisation, whereas hyperglycaemic conditions disrupt this process.

4.2.2.2 Effect of Glucose Concentration on 45S5 Bioactive Glass and CoSiBG (Low vs. Medium Glucose)

The greater mineralisation observed under low-glucose conditions compared to medium-glucose conditions in both 45S5 bioactive glass and CoSiBG is consistent with the supportive role of physiological glucose levels and obstructive role of hyperglycaemia in osteogenesis [24–27]. Between the two materials, 45S5 bioactive glass consistently exhibited slightly greater z-depths than CoSiBG, suggesting that its composition may provide a more favourable ionic environment for nucleation and growth of hydroxyapatite. This aligns with previous findings that 45S5 BG rapidly releases calcium and phosphate ions that accelerate mineralisation [30,31]. However, cobalt-containing glasses such as CoSiBG may exert additional modulatory effects that temper mineral deposition [32–34]. Overall, these findings highlight the importance of the metabolic environment and the influence of glass composition in regulating bone-like tissue mineralisation in vitro.

4.2.3 Effect of Biomaterial Composition

4.2.3.1 Effect of 45S5 Bioactive Glass and CoSiBG on Bone Mineralisation in Low Glucose (Physiologic) Conditions

Under low-glucose (physiological) conditions, mineralisation was slightly higher in the control compared to both 45S5 bioactive glass and CoSiBG. Ions released from bioactive glasses, such as calcium, phosphorus, and silicon, can support osteogenic activity by promoting osteoblast proliferation, stimulating alkaline phosphatase activity, and enhancing extracellular matrix mineral deposition [35]. However, under physiological conditions, osteoblasts already efficiently regulate mineralisation, and the ionic profile released from these glasses does not surpass the natural capacity of the cells. This

observation is consistent with previous studies showing that, although bioactive glass releases osteogenic ions, it lacks trace elements such as zinc and magnesium found in bone-derived hydroxyapatite, which further enhance mineralisation [36]. In addition, cobalt ions released from CoSiBG can influence cellular metabolism by stabilising hypoxia-inducible factor (HIF-1α), promoting angiogenic signalling, and in some cases inducing oxidative stress, which may interfere with optimal mineral deposition [32–34,37]. Clinical studies also suggest that ionic products from bioactive glasses support mineralisation but do not provide a significant advantage over the natural bone environment, which remains optimally suited for mineral deposition [38,39].

4.2.3.2 Effect of 45S5 Bioactive Glass and CoSiBG on Bone Mineralisation in Medium Glucose (Hyperglycaemic) Conditions

Under medium-glucose conditions, bulk mineralisation at lower magnifications was slightly lower in both 45S5 bioactive glass and CoSiBG compared to the control. At higher magnifications, both bioactive glasses supported mineral deposition to a similar extent as each other and the control, indicating that while bioactive glasses can maintain mineralisation under hyperglycaemic conditions, their contribution to large-scale mineral formation is slightly less than that of the native physiological environment. There is a lack of literature specifically examining the performance of 45S5 and CoSiBG under hyperglycaemic conditions. Other bioactive glasses, such as strontium- and lithium-doped variants, have been shown to favour mineralisation by creating an anti-inflammatory environment [40,41]. Whether 45S5 and cobalt-doped bioactive glass exert similar effects remains unknown and needs to be further investigated.

4.2.3.3 Comparison of 45S5 Bioactive Glass and CoSiBG

The slightly greater hydroxyapatite z-depth observed with 45S5 bioactive glass compared to CoSiBG suggests that 45S5 provides a more favourable environment for bulk mineral deposition. This observation is consistent with previous studies showing that copper can create a hypoxic microenvironment, which stimulates angiogenesis and wound healing but may partially impair osteogenesis [32–34,37]. At higher magnification, z-depths were comparable between the two materials, indicating that at the local cellular scale, both support similar osteogenic activity. These findings suggest that while material composition can influence overall mineralisation, differences are more apparent at larger tissue scales than at the level of individual cell layers. Both bioactive glasses likely provide sufficient ions locally for osteoblasts to deposit mineral at similar rates. However, over multiple cell layers and extended time, the cumulative effect of mineral deposition is greater for 45S5, resulting in thicker mineralised regions observable at lower magnifications but not at higher magnifications.

4.2.4 Effect of Culture Dimensionality (2D vs. 3D cultures)

The greater hydroxyapatite z-depth observed in 3D cultures compared to 2D reflects the enhanced osteogenic potential of three-dimensional environments. 3D culture better mimics the native bone microenvironment, providing improved cell–cell and cell–matrix interactions that support osteoblast differentiation and mineral deposition. These findings highlight the importance of culture dimensionality in promoting bone-like tissue development in vitro.

5 Conclusion

Confocal fluorescence microscopy, combined with the fluorescent probe OsteoImage™, provides a direct, specific, non-destructive, and cost-effective method for visualising and quantifying hydroxyapatite. This approach offers a straightforward tool with potential applications in evaluating biomaterials, assessing drug effects, and investigating disease mechanisms.

Acknowledgements

I want to express my sincere gratitude to my supervisor, Joel Turner, for his guidance, encouragement, and invaluable insights throughout this project. I am also grateful to Fidel Peacock for his support and assistance with the administrative aspects, which helped the research run smoothly. Finally, I would like to thank the Laidlaw Foundation for their generous funding, without which this work would not have been possible.

Bibliography

[1] O.A. Osuchukwu, A. Salihi, I. Abdullahi, B. Abdulkareem, C.S. Nwannenna, Synthesis techniques, characterization and mechanical properties of natural derived hydroxyapatite scaffolds for bone implants: a review, SN Applied Sciences 2021 3:10 3 (2021) 1–23. https://doi.org/10.1007/S42452-021-04795-Y.

[2] S. Mondal, S. Park, J. Choi, T.T.H. Vu, V.H.M. Doan, T.T. Vo, B. Lee, J. Oh, Hydroxyapatite: A journey from biomaterials to advanced functional materials, Adv Colloid Interface Sci 321 (2023) 103013. https://doi.org/10.1016/J.CIS.2023.103013.

[3] H. Shi, Z. Zhou, W. Li, Y. Fan, Z. Li, J. Wei, Hydroxyapatite Based Materials for Bone Tissue Engineering: A Brief and Comprehensive Introduction, Crystals 2021, Vol. 11, Page 149 11 (2021) 149. https://doi.org/10.3390/CRYST11020149.

[4] A.N. Tzavellas, C. Katrilaka, N. Karipidou, M. Kanari, M. Pitou, G. Koliakos, A. Cheva, T. Choli-Papadopoulou, A. Aggeli, E. Tsiridis, The “Forgotten” Hydroxyapatite

Crystals in Regenerative Bone Tissue Engineering: A Critical Review, Crystals (Basel) 14 (2024) 448. https://doi.org/10.3390/CRYST14050448/S1.

[5] Y. Shen, X. Huang, J. Wu, X. Lin, X. Zhou, Z. Zhu, X. Pan, J. Xu, J. Qiao, T. Zhang, L. Ye, H. Jiang, Y. Ren, P.F. Shan, The Global Burden of Osteoporosis, Low Bone Mass, and Its Related Fracture in 204 Countries and Territories, 1990-2019, Front Endocrinol (Lausanne) 13 (2022) 882241. https://doi.org/10.3389/FENDO.2022.882241/BIBTEX.

[6] A.M. Wu, C. Bisignano, S.L. James, G.G. Abady, A. Abedi, E. Abu-Gharbieh, R.K. Alhassan, V. Alipour, J. Arabloo, M. Asaad, W.N. Asmare, A.F. Awedew, M. Banach, S.K. Banerjee, A. Bijani, T.T.M. Birhanu, S.R. Bolla, L.A. Cámera, J.C. Chang, D.Y. Cho, M.T. Chung, R.A.S. Couto, X. Dai, L. Dandona, R. Dandona, F. Farzadfar, I. Filip, F. Fischer, A.A. Fomenkov, T.K. Gill, B. Gupta, J.A. Haagsma, A. Haj-Mirzaian, S. Hamidi, S.I. Hay, I.M. Ilic, M.D. Ilic, R.Q. Ivers, M. Jürisson, R. Kalhor, T. Kanchan, T. Kavetskyy, R. Khalilov, E.A. Khan, M. Khan, C.J. Kneib, V. Krishnamoorthy, G.A. Kumar, N. Kumar, R. Lalloo, S. Lasrado, S.S. Lim, Z. Liu, A. Manafi, N. Manafi, R.G. Menezes, T.J. Meretoja, B. Miazgowski, T.R. Miller, Y. Mohammad, A. Mohammadian-Hafshejani, A.H. Mokdad, C.J.L. Murray, M. Naderi, M.D. Naimzada, V.C. Nayak, C.T. Nguyen, R. Nikbakhsh, A.T. Olagunju, N. Otstavnov, S.S. Otstavnov, J.R. Padubidri, J. Pereira, H.Q. Pham, M. Pinheiro, S. Polinder, H. Pourchamani, N. Rabiee, A. Radfar, M.H. Ur Rahman, D.L. Rawaf, S. Rawaf, M.R. Saeb, A.M. Samy, L.S. Riera, D.C. Schwebel, S. Shahabi, M.A. Shaikh, A. Soheili, R. Tabarés-Seisdedos, M.R. Tovani-Palone, B.X. Tran, R.S. Travillian, P.R. Valdez, T.J. Vasankari, D.Z. Velazquez, N. Venketasubramanian, G.T. Vu, Z.J. Zhang, T. Vos, Global, regional, and national burden of bone fractures in 204 countries and territories, 1990–2019: a systematic analysis from the Global Burden of Disease Study 2019, Lancet Healthy Longev 2 (2021) e580–e592. https://doi.org/10.1016/S2666-7568(21)00172-0.

[7] J. Scheinpflug, M. Pfeiffenberger, A. Damerau, F. Schwarz, M. Textor, A. Lang, F. Schulze, Journey into Bone Models: A Review, Genes 2018, Vol. 9, Page 247 9 (2018) 247. https://doi.org/10.3390/GENES9050247.

[8] J. Hofmann, K. Borcherding, K. Thiel, T. Lingner, U. Sommer, U. Haberkorn, T.N. Bewersdorf, G. Schmidmaier, T. Grossner, ^{99m}Tc-HDP Labeling-A Non-Destructive Method for Real-Time Surveillance of the Osteogenic Differentiation Potential of hMSC during Ongoing Cell Cultures, Int J Mol Sci 23 (2022). https://doi.org/10.3390/ijms232415874.

[9] S.E. Doyle, D. Winrow, F. Buckley, E. Pernevik, M. Johnson, K. Thompson, L. Howard, C.M. Coleman, Optimization of 3D Extrusion-Printed Particle-Containing Hydrogels for Osteogenic Differentiation, ACS Omega 10 (2025) 15036–15051.

https://doi.org/10.1021/ACSOMEGA.4C10515/ASSET/IMAGES/LARGE/AO4C10515_0008.JPEG.

[10] L.M. Schäck, S. Noack, R. Winkler, G. Wissmann, P. Behrens, M. Wellmann, M. Jagodzinski, C. Krettek, A. Hoffmann, The Phosphate Source Influences Gene Expression and Quality of Mineralization during In Vitro Osteogenic Differentiation of Human Mesenchymal Stem Cells, PLoS One 8 (2013). https://doi.org/10.1371/journal.pone.0065943.

[11] E.E.A. Mohammed, H.H. Beherei, M. El-Zawahry, A.R.H. Farrag, N. Kholoussi, I. Helwa, M. Mabrouk, A.K.A. Aleem, Osteogenic enhancement of modular ceramic nanocomposites impregnated with human dental pulp stem cells: an approach for bone repair and regenerative medicine, JOURNAL OF GENETIC ENGINEERING AND BIOTECHNOLOGY 20 (2022). https://doi.org/10.1186/s43141-022-00387-4.

[12] S.S. Kim, M.S. Park, O. Jeon, C.Y. Choi, B.S. Kim, Poly(lactide-co-glycolide)/hydroxyapatite composite scaffolds for bone tissue engineering, Biomaterials 27 (2006) 1399–1409. https://doi.org/10.1016/j.biomaterials.2005.08.016.

[13] I. Pignatelli, A. Kumar, K. Shah, M. Balonis, M. Bauchy, B. Wu, G. Sant, Vertical scanning interferometry: A new method to quantify re-/de-mineralization dynamics of dental enamel, DENTAL MATERIALS 32 (2016) E251–E261. https://doi.org/10.1016/j.dental.2016.07.004.

[14] Y.U. Hanim, S. Ebrahimi, A.J. Norsazlina, P.C. Lee, P.L. Teoh, S.E. Arshad, C.S. Sipaut, S.E. How, Evaluation of human amnion denuded derived mesenchymal stem cell on 3D porous hydroxyapatite composite scaffolds for osteogenic differentiation: Prolonged in vitro study, JOURNAL OF SCIENCE-ADVANCED MATERIALS AND DEVICES 8 (2023). https://doi.org/10.1016/j.jsamd.2023.100636.

[15] B. De Vega, A. Dutta, A. Mumtaz, B.C. Schroeder, C. Gerrand, A.S. Boyd, D.M. Kalaskar, Comparative analysis of solvent-based and solvent-free (melting) methods for fabricating 3D-printed polycaprolactone-hydroxyapatite composite bone scaffolds: physicochemical/mechanical analyses and in vitro cytocompatibility, Front Bioeng Biotechnol 12 (2024) 1473777. https://doi.org/10.3389/FBIOE.2024.1473777/BIBTEX.

[16] A. Giuliani, M.L. Gatto, L. Gobbi, F.G. Mangano, C. Mangano, Integrated 3D Information for Custom-Made Bone Grafts: Focus on Biphasic Calcium Phosphate Bone Substitute Biomaterials, Int J Environ Res Public Health 17 (2020). https://doi.org/10.3390/ijerph17144931.

[17] G.R. Davis, A.N.Z. Evershed, D. Mills, Quantitative high contrast X-ray microtomography for dental research, J Dent 41 (2013) 475–482. https://doi.org/10.1016/j.jdent.2013.01.010.

[18] M. Fuerst, L. Lammers, F. Schäfer, O. Niggemeyer, J. Steinhagen, C.H. Lohmann, W. Rüther, Investigation of calcium crystals in OA knees, Rheumatol Int 30 (2010) 623–631. https://doi.org/10.1007/s00296-009-1032-2.

[19] T. Grossner, U. Haberkorn, T. Gotterbarm, ¹⁸F- based Quantification of the Osteogenic Potential of hMSCs, Int J Mol Sci 21 (2020). https://doi.org/10.3390/ijms21207692.

[20] E. Kaivosoja, V. Sariola, Y. Chen, Y.T. Konttinen, The effect of pulsed electromagnetic fields and dehydroepiandrosterone on viability and osteo-induction of human mesenchymal stem cells, J Tissue Eng Regen Med 9 (2015) 31–40. https://doi.org/10.1002/TERM.1612.

[21] P.B. Kasi, A. Serafin, L. O'Brien, N. Moghbel, L.N. Novikov, P. Kelk, M.N. Collins, Electroconductive gelatin/hyaluronic acid/hydroxyapatite scaffolds for enhanced cell proliferation and osteogenic differentiation in bone tissue engineering, Biomaterials Advances 173 (2025) 214286. https://doi.org/10.1016/J.BIOADV.2025.214286.

[22] L.F. Pettersson, P.J. Kingham, M. Wiberg, P. Kelk, In Vitro Osteogenic Differentiation of Human Mesenchymal Stem Cells from Jawbone Compared with Dental Tissue, Tissue Eng Regen Med 14 (2017) 763–774. https://doi.org/10.1007/S13770-017-0071-0/FIGURES/7.

[23] V. Zymovets, O. Rakhimova, P. Wadelius, A. Schmidt, M. Brundin, P. Kelk, M. Landström, N.R. Vestman, Exploring the impact of oral bacteria remnants on stem cells from the Apical papilla: mineralization potential and inflammatory response, Front Cell Infect Microbiol 13 (2023) 1257433. https://doi.org/10.3389/FCIMB.2023.1257433/XML/NLM.

[24] J.S. Cunha, V.M. Ferreira, E. Maquigussa, M.A. Naves, M.A. Boim, Effects of high glucose and high insulin concentrations on osteoblast function in vitro, Cell Tissue Res 358 (2014) 249–256. https://doi.org/10.1007/S00441-014-1913-X/FIGURES/5.

[25] S. Fujimori, M. Osawa, M. Iemata, E. Hinoi, Y. Yoneda, Increased GABA Transport Activity in Rat Calvarial Osteoblasts Cultured under Hyperglycemic Conditions, Biol. Pharm. Bull 29 (2006) 297–301.

[26] L. Entz, G. Falgayrac, C. Chauveau, G. Pasquier, S. Lucas, The extracellular matrix of human bone marrow adipocytes and glucose concentration differentially alter mineralization quality without impairing osteoblastogenesis, Bone Rep 17 (2022) 101622. https://doi.org/10.1016/J.BONR.2022.101622.

[27] V. Gopalakrishnan, R.C. Vignesh, J. Arunakaran, M.M. Aruldhas, N. Srinivasan, Effects of glucose and its modulation by insulin and estradiol on BMSC differentiation into osteoblastic lineages, Biochemistry and Cell Biology 84 (2006) 93–101. https://doi.org/10.1139/O05-163.

[28] L.L. Ramenzoni, A. Bösch, S. Proksch, T. Attin, P.R. Schmidlin, Effect of high glucose levels and lipopolysaccharides-induced inflammation on osteoblast mineralization over sandblasted/acid-etched titanium surface, Clin Implant Dent Relat Res 22 (2020) 213–219. https://doi.org/10.1111/CID.12884;PAGE:STRING:ARTICLE/CHAPTER.

[29] H. Kato, Y. Taguchi, K. Tominaga, D. Kimura, I. Yamawaki, M. Noguchi, N. Yamauchi, I. Tamura, A. Tanaka, M. Umeda, High Glucose Concentrations Suppress the Proliferation of Human Periodontal Ligament Stem Cells and Their Differentiation Into Osteoblasts, J Periodontol 87 (2016) e44–e51. https://doi.org/10.1902/JOP.2015.150474;PAGE:STRING:ARTICLE/CHAPTER.

[30] A. Pizzi, Y. Li, M. Zou, J.-W. Choi, A.R. Han, S.-Y. Yang, Ion Release and Apatite Formation of Resin Based Pit and Fissure Sealants Containing 45S5 Bioactive Glass, Polymers 2024, Vol. 16, Page 1855 16 (2024) 1855. https://doi.org/10.3390/POLYM16131855.

[31] Z. Jin, D.R. Neuville, D.S. Brauer, Glasses for bone regeneration: structural features controlling physical properties and ion release of bioactive glasses 45S5, S53P4 and 13-93, RSC Adv 15 (2025) 4997–5006. https://doi.org/10.1039/D4RA06081D.

[32] L. Soltani, K. Varmira, M. Nazari, Comparison of the differentiation of ovine fetal bone-marrow mesenchymal stem cells towards osteocytes on chitosan/alginate/CuO-NPs and chitosan/alginate/FeO-NPs scaffolds, Sci Rep 14 (2024) 1–23. https://doi.org/10.1038/S41598-023-50664-6;SUBJMETA=301,532,631,639,80;KWRD=CELL+BIOLOGY,MATERIALS+SCIENCE,STEM+CELLS.

[33] G.P. Tabari, M.M. Keshtiban, K.N. Osguei, S.A. Injectable Hydrogel, Correction to “Injectable Hydrogel Scaffold Incorporating Microspheres Containing Cobalt-Doped Bioactive Glass for Bone Healing,” J Biomed Mater Res A 113 (2025) e37910. https://doi.org/10.1002/JBM.A.37910.

[34] Z. Deng, B. Lin, Z. Jiang, W. Huang, J. Li, X. Zeng, H. Wang, D. Wang, Y. Zhang, Hypoxia-Mimicking Cobalt-Doped Borosilicate Bioactive Glass Scaffolds with Enhanced Angiogenic and Osteogenic Capacity for Bone Regeneration, Int J Biol Sci 15 (2019) 1113–1124. https://doi.org/10.7150/IJBS.32358.

[35] N. Gómez-Cerezo, L. Casarrubios, I. Morales, M.J. Feito, M. Vallet-Regí, D. Arcos, M.T. Portolés, Effects of a mesoporous bioactive glass on osteoblasts, osteoclasts

and macrophages, J Colloid Interface Sci 528 (2018) 309–320. https://doi.org/10.1016/j.jcis.2018.05.099.

[36] A. Doostmohammadi, A. Monshi, M.H. Fathi, O. Braissant, A comparative physico-chemical study of bioactive glass and bone-derived hydroxyapatite, Ceram Int 37 (2011) 1601–1607. https://doi.org/10.1016/J.CERAMINT.2011.03.009.

[37] J.R. de Souza, C. Anselmi, L.M. Cardoso, L.T. Kito, A.H. dos Reis-Prado, P.H.C. de Oliveira, R. Dal-Fabbro, M. Rahimnejad, T.M.B. Campos, L.T.A. Cintra, A.L.S. Borges, M.C. Bottino, Electrospun SilkMA/silicate-chlorinated cobalt-doped bioactive glass composite for bone regeneration, J Mech Behav Biomed Mater 164 (2025) 106929. https://doi.org/10.1016/J.JMBBM.2025.106929.

[38] E. Steinhausen, R. Lefering, M. Glombitza, N. Brinkmann, C. Vogel, B. Mester, M. Dudda, Bioactive glass S53P4 vs. autologous bone graft for filling defects in patients with chronic osteomyelitis and infected non-unions – a single center experience, J Bone Jt Infect 6 (2021) 73. https://doi.org/10.5194/JBJI-6-73-2021.

[39] H.T. Aro, V.V. Välimäki, N. Strandberg, P. Lankinen, E. Löyttyniemi, V. Saunavaara, M. Seppänen, Bioactive glass granules versus standard autologous and allogeneic bone grafts: a randomized trial of 49 adult bone tumor patients with a 10-year follow-up, Acta Orthop 93 (2022) 519–527. https://doi.org/10.2340/17453674.2022.2808.

[40] Z. Xu, X. Qi, M. Bao, T. Zhou, J. Shi, Z. Xu, M. Zhou, A.R. Boccaccini, K. Zheng, X. Jiang, Biomineralization inspired 3D printed bioactive glass nanocomposite scaffolds orchestrate diabetic bone regeneration by remodeling micromilieu, Bioact Mater 25 (2023) 239–255. https://doi.org/10.1016/J.BIOACTMAT.2023.01.024.

[41] Z. Wu, J. Bai, G. Ge, T. Wang, S. Feng, Q. Ma, X. Liang, W. Li, W. Zhang, Y. Xu, K. Guo, W. Cui, G. Zha, D. Geng, Regulating Macrophage Polarization in High Glucose Microenvironment Using Lithium-Modified Bioglass-Hydrogel for Diabetic Bone Regeneration, Adv Healthc Mater 11 (2022) 2200298. https://doi.org/10.1002/ADHM.202200298;REQUESTEDJOURNAL:JOURNAL:21922659.